EARLY ASSESSMENT OF MALIGNANT LUNG NODULES BASED ON THE SPATIAL ANALYSIS OF DETECTED LUNG NODULES

A. El-Baz[1*], *A. Soliman*[1], *P. McClure*[1], *G. Gimel'farb*[2], *M. Abo El-Ghar*[3], *R. Falk*[4]

[1] BioImaging Lab, Bioengineering Department, University of Louisville, Louisville, KY, USA
[2]Department of Computer Science, The University of Auckland, Auckland, New Zealand.
[3]Urology and Nephrology Department, University of Mansoura, Mansoura, Egypt.
[4]Department of Radiology, Jewish Hospital, Louisville, KY, USA.

ABSTRACT

We propose a novel approach for diagnosing malignant lung nodules based on analyzing the spatial distribution of Hounsfield values for the detected lung nodules. Spatial distribution of image intensities (or Hounsfield values) comprising the malignant nodule appearance is accurately modeled with a new rotationally invariant second-order Markov-Gibbs Random Field (MGRF). In this paper, we introduce a new maximum likelihood estimation approach to estimate the neighborhood system of the proposed rotation invariant MGRF and its potentials from a training set of nodule images with normalized intensity ranges. Preliminary experiments on 327 lung nodules (153 malignant and 174 benign) resulted in the 91.1% correct classification (for the 95% confidence interval), showing the proposed method is a promising supplement to current technologies (biopsy-based diagnostic systems) for the early diagnosis of lung cancer.

Index Terms— Lung nodules, CT, Markov fields.

1. INTRODUCTION

Pulmonary nodules are frequently found during computed tomography (CT) scans of the chest area [1]. The improvement in resolution and the broad availability of spiral and multi-detector row CTs has resulted in an increasing number of pulmonary nodules being detected [1]. The goal of a radiological evaluation of small pulmonary nodules is to differentiate between benign and malignant lesions at an early stage.

Large malignant nodules (generally defined as greater than 1 cm in diameter) are easily detected with any traditional imaging equipment and are then diagnosed by needle biopsy or bronchoscopy. However, diagnostic options for small malignant nodules are limited due to difficulties in their accessibility, especially if they are located deep in the tissue or away from large airways. Therefore, additional imaging and Computer-Aided Diagnostic (CAD) systems are needed.

Previous work. Volumetric-based analysis approaches of doubling time are increasingly being tested and have been proven in studies to correlate with the benign or malignant nature of nodules [2, 3, 4]. Tracking the temporal nodule behavior is a challenging task due to changes in the patient's position at each data acquisition and the effects of the patient's heart beat and respiration. In order to accurately measure how the nodules develop over time, these motions should be compensated for by registering the Low Dose Computed Tomography (LDCT) data sets taken at different time points. Many methods have been proposed for solving medical image registration problems (see e.g. [5]) and excluding the lung motions [6]. Moreover, it has been reported that computer-assisted volume measurements are more reliable for small pulmonary nodules than the measurements made by human experts [7]. Even with these techniques, the accuracy of nodule classification based on the growth rate remains below clinical requirements [7]. *To the best of our knowledge, this paper is the first to characterize the detected nodules by modeling and analyzing their visual appearance (spatial distribution of Hounsfield values of the lung nodule voxels). Such an analysis does not involve image registration.*

2. METHODS

In this work, we propose a novel appearance-based approach for the analysis of the lung nodules' appearance variability between malignant and benign nodules (See Fig. 1). *In this paper we will focus on steps 3 and 4. The first two steps are shown in detail in [8, 9].*

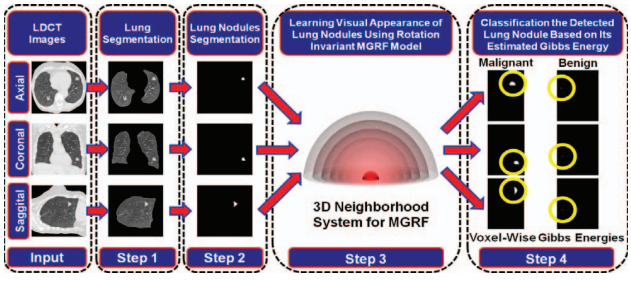


Fig. 1. Proposed appearance-based system for early assessment of malignant nodules.

*Corresponding author:- Tel:(502)-852-5092, Fax:(502)-852-6806, E-mail: aselba01@louisville.edu

2.1. MGRF-based prior appearance model

The visual appearance of both the small 2D and the large 3D malignant lung nodules in an LDCT chest image are modeled with a generic translation and rotation invariant second-order MGRF. Its voxel-wise and central-symmetric pairwise voxel potentials account for differences between the Hounsfield values (i.e. gray levels, or intensities) of the nodules. Possible monotone (order-preserving) intensity changes, e.g. due to different sensor characteristics, are taken into account by equalizing [10] lung areas on every segmented LDCT data set.

Figure 2 presents axial cross-sections of two lung nodules suggesting that the spatial distribution of the Hounsfield values is considerably less smooth for a malignant nodule compared to a benign one. The MGRF model describes peculiarities in the visual appearance of the malignant nodules in terms of pairwise spatial co-occurrences of the equalized Hounsfield values.

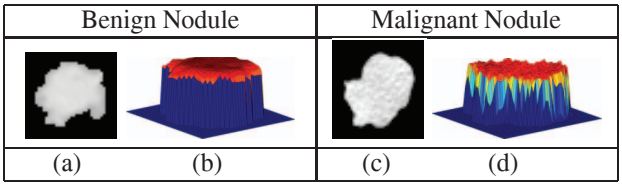


Fig. 2. 2D (a,c) and 3D (b,d) visualization of Hounsfield values over an axial cross-section of a benign and malignant nodule.

Let (x, y, z) be Cartesian point coordinates in a 3D lattice $\mathbf{R} = [(x, y, z) : x = 0, \ldots, X-1; y = 0, \ldots, Y-1, z = 1, \ldots, Z-1]$ supporting 3D images $\mathbf{g} = [g_{x,y,z} : (x, y, z) \in \mathbf{R}; g_{x,y,z} \in \mathbf{Q}]$ with a finite set of intensities $\mathbf{Q} = \{0, \ldots, Q-1\}$. The translation and rotation invariant MGRF is specified by a set $\mathbf{N}$ of characteristic central-symmetric voxel neighborhoods $\{\mathbf{n}_\nu : \nu \in \mathbf{N}\}$ on $\mathbf{R}$ shown in Fig. 3. Let $V_{\boldsymbol{\nu}} : \mathbf{D} \to \mathbf{R} = (-\infty, \infty)$, where $\mathbf{D} = \{-Q+1, \ldots, 0, 1, \ldots, Q-1\}$ is the set of pairwise signal differences, and denotes a real-valued Gibbs potential function for the neighboring voxel pairs with the relative coordinate offset $\boldsymbol{\nu}$. Each such pair is a second-order clique of the neighborhood graph. All the cliques are stratified into $\mathbf{C}$ families, $\mathbf{C}_{\boldsymbol{\nu}} = \{\mathbf{c}_{\boldsymbol{\nu}} : \nu \in \mathbf{R}\}$, of translation invariant cliques having the same interaction potential $V_{\boldsymbol{\nu}}$ taking $2Q-1$ values, which can be represented in the vectorial form: $\mathbf{V}_{\boldsymbol{\nu}} = [V_{\boldsymbol{\nu}}(\Delta) : \Delta \in \mathbf{D}]$.

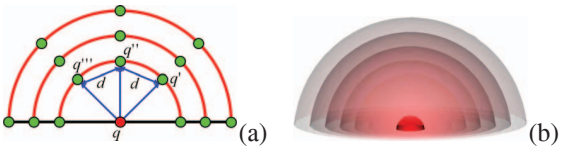


Fig. 3. Central-symmetric second-order 2D (a) and 3D (b) neighborhood system.

A generic translation and rotation invariant second-order Markov-Gibbs random field (MGRF) of images $\mathbf{g} = (g(x, y, z) : (x, y, z) \in \mathbf{R})$, which is invariant to image translations, rotations and global signal offsets, has the following Gibbs probability distribution (GPD):

$$P(\mathbf{g}|\mathbf{V}) = \frac{1}{Z_{\mathbf{V}}} \exp\left(|\mathbf{R}| \sum_{\nu \in \mathbf{N}} \rho_\nu \mathbf{V}_\nu^{\mathsf{T}} \mathbf{F}_\nu(\mathbf{g})\right) \quad (1)$$

where $Z_{\mathbf{V}}$ is the normalizing factor (called the partition function) for potentials $\mathbf{V} = [\mathbf{V}_{\boldsymbol{\nu}} : \boldsymbol{\nu} \in \mathbf{N}]$ for a certain neighborhood $\mathbf{N}$, $\rho_\nu = \frac{|\mathbf{C}_\nu|}{|\mathbf{R}|}$ is the relative size of the clique family with respect to the lattice cardinality $|\mathbf{R}| = X \times Y \times Z$, i.e. the relative number of cliques in the clique family $\mathbf{C}_{\boldsymbol{\nu}}$); T indicates the vectorial transposition, and the vector $\mathbf{F}_\nu(\mathbf{g}) = \left[f_\nu(\Delta|\mathbf{g}) = \frac{|\mathbf{C}_{\nu:\Delta}(\mathbf{g})|}{|\mathbf{C}_\nu|}; \sum_{\Delta \in \mathbf{D}} f_\nu(\Delta|\mathbf{D}) = 1\right]$ contains relative frequencies of signal differences $\Delta \in \mathbf{D}$ in the cliques from the family $\mathbf{C}_{\boldsymbol{\nu}}$ for the image $\mathbf{g}$, the subfamily $\mathbf{C}_{\boldsymbol{\nu}:\Delta}(\mathbf{g})$ containing all the cliques of this family, such that $g(x, y, z) - g(x', y', z') = \Delta$.

The central-symmetric voxel neighborhood $\mathbf{n}_\nu$ embraces all voxel pairs such that the coordinate offsets between any voxel (x, y, z) and its neighbor (x', y', z') belong to an indexed semi-open interval $[d_{\nu,\min}, d_{\nu,\max})$; $\nu \in \mathbf{N} \subset \{1, 2, 3, \ldots\}$ of the inter-voxel distances:

$$d_{\nu,\min} \leq \sqrt{(x-x')^2 + (y-y')^2 + (z-z')^2} < d_{\nu,\max}. \quad (2)$$

Figure 3(a) illustrates the neighborhoods for the distance ranges $d_{\nu,\min} = \nu - 0.5$ and $d_{\nu,\max} = \nu + 0.5$; $\nu \in \mathbf{N} = \{1, \ldots, 4\}$.

Each neighborhood $\mathbf{n}_\nu$ has the same potential function $\mathbf{V}_\nu$ of the absolute intensity difference $\Delta = |q - q'|$ between the neighboring voxel pairs: $\mathbf{V}_\nu = (V_\nu(\Delta) : \Delta \in \mathbf{D}$, where $q = g(x, y, z)$; $q' = g(x', y', z')$, and $\mathbf{D} \equiv \mathbf{Q} = \{0, 1, \ldots, Q-1\}$. The voxel potential $\mathbf{V}_{\text{vox}} = (V_{\text{vox}}(q) : q \in \mathbf{Q})$ depends on the voxel intensities.

In this paper, we introduce a new maximum likelihood analytical approach to estimate the potentials of a Markov-Gibbs Random Field (MGRF) (Please see the supplementary material for the complete proof). The potentials are analytically approximated as:

$$V_\nu(\Delta) = \lambda\left(f_\nu(\Delta) - f_{\text{irf}}(\Delta)\right); \nu \in \mathbf{N} \quad (3)$$

where $f_\nu(\Delta)$ is the empirical probability of the pairwise intensity difference Δ for the voxel pairs corresponding to the neighborhood $\mathbf{n}_\nu$ over the training data set; $f_{\text{irf}}(\Delta)$ denotes the probability of the same difference Δ for the independent random field of equiprobable intensities:

$$f_{\text{irf}}(\Delta) = \begin{cases} \frac{1}{Q} & \text{if } \Delta = 0 \\ \frac{2(Q-\Delta)}{Q^2} & \text{otherwise} \end{cases}$$

and the common factor λ is also computed analytically. Below it is omitted ($\lambda = 1$) because only relative potentials are used for computing relative energies $E_{\nu,\text{rel}}$ of the neighborhoods.

Neighborhood Selection: The relative energies:

$$E_{\nu,\mathrm{rel}} = \sum_{\Delta \in \mathbf{D}} f_\nu(\Delta)\left(f_\nu(\Delta) - f_{\mathrm{irf}}(\Delta)\right) \qquad (4)$$

allow for the ranking of all the available neighborhoods $\mathbf{n}_\nu$ and selecting the characteristic subset $\mathbf{N}$ for the prior MGRF appearance model with the potentials of Eq. (3).

Under the learned model, any nodule image $\mathbf{g}$ is described by its Gibbs energy

$$E(\mathbf{g}) = \mathbf{V}_{\mathrm{vox}}^{\mathsf{T}}\mathbf{F}_{\mathrm{vox}}(\mathbf{g}) + \sum_{\nu \in \mathbf{N}} \rho_\nu \mathbf{V}_\nu^{\mathsf{T}}\mathbf{F}_\nu(\mathbf{g}) \qquad (5)$$

where $\mathbf{N}$ is a set of the selected neighbors, $\mathbf{F}_{\mathrm{vox}}(\mathbf{g})$ and $\mathbf{F}_\nu(\mathbf{g})$ are vectors of the empirical probability distributions of intensities and absolute intensity differences collected within the nodule in $\mathbf{g}$, and ρ_ν denotes a relative cardinality of the set of all the voxel pairs corresponding to the neighborhood ν with respect to the lattice cardinality $X \times Y \times Z$.

3. EXPERIMENTAL RESULTS

To justify the proposed methodology of learning the 3D appearance (i.e. spatial distribution of Hounsfield values) of both malignant and benign nodules after normalizing the image signals, the above appearance analysis was tested on a database of clinical multislice 3D chest LDCT scans of 327 lung nodules (153 malignant and 174 benign). The scanned CT data sets each have $0.7 \times 0.7 \times 2.0$ mm^3 voxels, with the diameters of the nodules ranging from 3 mm to 30 mm. Note that these 327 nodules were diagnosed using either a bronchoscopy and needle biopsy, or a two-year follow-up with CT scans. Note that the small nodules (less than 10 mm in diameter) were diagnosed by two-year follow-up with CT scans.

In order to illustrate the significance of our methodology of learning the 3D appearance (spatial distribution of Hounsfield values) of both malignant and benign nodules after handling all of the motion artifacts due to breathing and heart beating, we performed unpaired t-test. Table 1 shows Gibbs energies for both a malignant and a benign nodule. It suggests that the energy of a malignant nodule is higher than that of a benign nodule; this encourages the use of the Gibbs energy as a discriminatory feature to distinguish malignant from benign nodules. Table VIII shows the average Gibbs energy of the malignant and benign nodules.

As demonstrated in Fig. 4, the probability distributions of the average Gibbs energy over each detected lung nodule used to describe the 3D appearance of 50 malignant and 58 benign nodules were obtained using a close approximation of the empirical mixture using the approach in [9]. Note that the average Gibbs energy is estimated by averaging all of the voxel–wise Gibbs energies, which are calculated using Eq. 5 for each detected lung nodule.

The training subset for classification (30 malignant lung nodules and 30 benign lung nodules) was arbitrarily selected

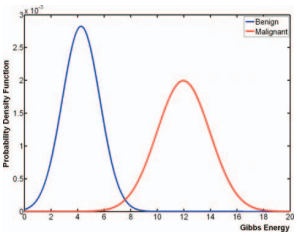


Fig. 4. Energy probability models describing the appearance of 3D malignant and benign nodules

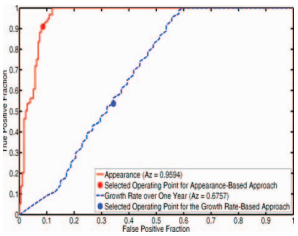


Fig. 5. The ROC curves for the proposed approach and the growth rate based diagnostic approach.

from among all of the 327 lung nodules. The classification accuracy of a Bayes classifier using the estimated probability models in Fig. 4 was evaluated using the χ^2-test at 95% confidence level. At the 95% confidence level, 139 out of 153 malignant nodules (a 90.8% accuracy), and 159 out of 174 control subjects (a 91.3% accuracy) were correctly classified. The overall accuracy using the proposed 3D appearance-based CAD system for 95% confidence level is 91.1% during the first detection of lung nodules.

The advantages of using the proposed 3D appearance-based CAD system are highlighted by comparing the accuracy of our system to that of the approach proposed by Reeves et al. [11], which is based on the estimation of a lung nodule growth rate over a one year time frame from the first detection. It has been shown that using the proposed 3D appearance-based CAD system leads to an accuracy of 91.1%. On the other hand, classification based on traditional growth rate approaches [11] over one year is 87 out of 153 for malignant nodules (a 56.9% accuracy), and 114 out of 174 for benign nodules (a 65.7% accuracy) at a 95% confidence level.

Moreover, we compared the diagnostic with the standard deviation which is a standard method for measuring global intensity homogeneity in the detected lung nodules. The classification based on using the standard deviation is 55 out of 153 for malignant nodules (a 35.9% accuracy), and 79 out of 174 for benign nodules (a 45.4% accuracy) at a 95% confidence level. The low accuracy of standard deviation based-classification method is due to the fact that the standard deviation measures only the global homogeneity and therefore is of limited value for the spatial appearance analysis. Intensity variations between the near neighbors by themselves are too noisy, resulting in characteristics of homogeneity with very limited descriptive power. But these variations are taken into account and integrated in the proposed MGRF energy with a large set of other characteristic close- and long-range intensity variations. This is why the proposed energy outperforms simpler measures of local homogeneity.

Another way to measure and test the performance of the proposed diagnostic system is to compute the receiver operating characteristic (ROC). Each point on the graph is generated by using a different cut point (classification threshold). Figure 5 shows the ROC of the two approaches, our proposed

Table 1. Statistical analysis of the Gibbs energy of lung nodules detected for the 30 malignant nodules and 30 benign nodules. Note that μ stands for the mean, σ stands for the standard deviation, B stands for benign nodules, and M stands for malignant nodules

Scanning period	**Malignant Nodules**		Benign Nodules		**Statistical significance**
	$\mu_M(\%)$	$\sigma_M(\%)$	$\mu_B(\%)$	$\sigma_B(\%)$	p-value
3 months	33.24	2.12	8.10	0.97	0.0001
6 months	37.59	2.22	8.91	0.81	0.0001
9 months	39.16	3.19	9.01	0.86	0.0001
12 months	41.91	3.29	9.06	0.91	0.0001

appearance-based diagnostic approach and the growth rate based diagnostic approach [11]. It is clear from Fig. 5 that the area under the ROC curve of our present approach is larger (Az = 0.9594) than the area under the ROC of the growth rate based diagnostic approach [11] (Az is 0.6757 for one year estimated growth rate). The high sensitivity and specificity of the proposed approach is due to using the estimated Gibbs energy of the detected lung nodule as a new discriminatory feature that has the ability to describe the appearance variability between malignant and benign nodules. This new discriminatory feature is more separable than using the estimated growth rate.

4. CONCLUSIONS

The preliminary results shown in this paper justify the elaboration of the proposed alternative method for diagnosing malignant lung nodules. Its novelty lies in using the appearance of a segmented 3D nodule instead of the more conventional growth rate as a reliable diagnostic feature. The appearance is described in terms of the voxel-wise conditional Gibbs energies for a generic rotationally and translationally invariant second-order MGRF model of malignant nodules with analytically estimated characteristics for voxel neighborhoods and potentials.

The proposed nodule appearance analysis could lead to faster, more accurate, and more useful clinical diagnostics for detecting pulmonary nodules without the need for investigating their temporal development on successive LDCT images of the same subject collected over a relatively long time. The present C++ implementation on the Intel quad processor (3.2GHz each) with 16 GB memory and 1.5 TB hard drive with the RAID technology takes approximately 5 sec for processing 30 mm lung nodules and less than 1 sec for processing 5mm lung nodules.

Acknowledgment: This research work has been supported by Research Scholar Grants, 120556-RSG-11-266-01-CCE, from the American Cancer Society.

5. REFERENCES

[1] S. J. Swensen, et al., "Screening for lung cancer with low-dose spiral computed tomography," *Am J Respir Crit Care Med*, vol. 165, no. 4, pp. 508-13, 2002.

[2] C. Hui, W. Xiao-hua, M. Da-qing and M. Bin-rong, "Neural network-based computer-aided diagnosis in distinguishing malignant from benign solitary pulmonary nodules by computed tomography," *Chin Med J (Engl)*, vol. 120, no. 14, pp. 1211-1215, 2007.

[3] S. Sone, K. Tsushima, K. Yoshida, K. Hamanaka, T. Hanaoka and R. Kondo, "Pulmonary nodules: Preliminary experience with semiautomated volumetric evaluation by CT stratum," *Acad Radiol*, vol. 17, no. 7, pp. 900-911, 2010.

[4] M. Revel, C. Lefort, A. Bissery, M. Bienvenu, L. Aycard, G. Chatellier, G. Frija, "Pulmonary nodules: preliminary experience with three-dimensional evaluation," Radiology, 2004. vol. 231, no. 2, pp. 459-466.

[5] J. Maintz and M. Viergever, "A Survey of Medical Image Registration," *Journal of Medical Image Analysis*, vol. 2, pp. 1–36, 1998.

[6] J. Ko and D. Naidich, "Computer-Aided Diagnosis and the Evaluation of Lung Disease," *Journal of Thoracic Imaging*, vol. 19, no. 3, pp. 136–155, 2004.

[7] W. Kostis, D. Yankelevitz, A. Reeves, S. Fluture, C. Henschke, "Small Pulmonary Nodules: Reproducibility of Three-dimensional Volumetric Measurement and Estimation of Time to Follow-up CT," *Radiology*, vol. 231, pp. 446-452, May 2004.

[8] A. El-Baz, M. Nitzken, F. Khalifa, A. Elnakib, G. Gimelfarb, R. Falk, and M. Abo El-Ghar, 3D Shape Analysis for Early Diagnosis of Malignant Lung Nodules, *IPMI'11*, Monastery Irsee, Germany, July 3-8, 2011. pp. 772-783.

[9] A. El-Baz, G. Gimelfarb, R. Falk, M. Abou El-Ghar, Holland, and T. Shaffer, "A New Stochastic Framework for Accurate Lung Segmentation," *MICCAI'08*, New York, USA, September 6 - 10, 2008, pp. 322-330.

[10] R. Gonzalez and R. Woods, *Digital Image Processing,* Addison- Wesley Publishing Company (New York), 1992.

[11] A. Reeves, A. Chan, D. Yankelevitz, C. Henschke, B. Kressler, and W. Kostis, "On Measuring the Change in Size of Pulmonary Nodules," *IEEE Transactions on Medical Imaging*, vol. 25, no. 4, pp. 435–449, April 2006.